nature structural & molecular biology

Brief Communication

https://doi.org/10.1038/s41594-026-01894-5

Architecture of a DNA-guided Cas12a

Received: 21 March 2026

Accepted: 26 August 2026

Published online: 09 September 2026

Check for updates

Rodrigo Fregoso Ocampo[1,2,9], Carlos Orosco[3,9], Boyu Huang[3], Madeline S. West[1], Bay Parker[4], Piyush K. Jain[3,5,6] ✉ & David W. Taylor[1,2,7,8] ✉

CRISPR–Cas systems have largely been restricted to RNA-guided nucleases. Here, we present the cryo-electron microscopy structure of *Acidaminococcus* sp. Cas12a bound to a pseudo-DNA (ΨDNA) guide and RNA target, revealing how Cas12a can accomplish DNA-guided RNA recognition. The ΨDNA hairpin bridges the recognition and nuclease lobes, mimicking a PAM-proximal duplex and positioning the spacer to allow formation of a canonical RNA–DNA heteroduplex along the recognition lobe. This provides a structural framework for its activity and provides a potential blueprint for future engineering.

CRISPR–Cas systems function as prokaryotic adaptive immune modules, using sequence-guided nucleic acid target recognition. Beyond their biological role, these systems have been repurposed as versatile platforms for genome engineering in both fundamental research and therapeutic applications[1,2]. CRISPR–Cas systems are canonically RNA-guided enzymes that direct programmable recognition of target sequences. Cas12a, a class 2 type V system, typically uses a CRISPR RNA (crRNA) guide that directs cleavage of double-stranded DNA (dsDNA) targets containing a protospacer-adjacent motif (PAM)[3,4]. Although several CRISPR nucleases have been adapted for RNA targeting[5–8], this activity generally relies on an RNA guide and possess nonspecific collateral cleavage activity on bystander RNAs. Recent work from our group introduced a DNA-guided Cas12a repurposed to recognize RNA targets with high specificity using engineered pseudo-DNA (ΨDNA) guides[9]. However, how Cas12a structurally accommodates a DNA guide while recognizing an RNA substrate remained unknown. Here, we determined the cryo-electron microscopy (cryo-EM) structure of *Acidaminococcus* sp. Cas12a (AsCas12a) bound to a ΨDNA guide and RNA target at 3.18-Å resolution, revealing how Cas12a accommodates an RNA target through structural mimicry of canonical CRISPR components (PDB 12YR) (Fig. 1a, Table 1 and Extended Data Fig. 1).

Structure of DNA-guided AsCas12a

Our structure adopts the canonical bilobed architecture, resembling previously reported Cas12a structures in complex with crRNA and dsDNA targets[10,11]. Surprisingly, the ΨDNA hairpin bridges the two lobes and binds the PID and WED domains in the same position that the PAM-proximal dsDNA helix would be recognized in RNA-guided systems[12] (Fig. 1a). The design of the ΨDNA, which contains a 3′-hairpin or handle and 5′-spacer, enables AsCas12a to bind the hairpin in the same directionality that it would bind a canonical dsDNA target duplex. This positions the ΨDNA spacer where the target strand (TS) would be in a canonical R-loop and with the same directionality (Fig. 1b). This structure explains our recent findings that show that a 5′ handle is much less active than a 3′ handle, as this geometry of nucleic acids would be incompatible within this structural framework. In addition, the structure suggests that a dual handle ΨDNA with both a 5′ and a 3′ hairpin would not notably affect activity, as we reported. In this case, the 3′ handle would be properly recognized, the spacer would traverse through the enzyme and the 5′ handle would be located outside of the core on the recognition lobe 2 (REC2) end of the enzyme. Together, this indicates that the ΨDNA architecture uniquely recreates the spatial cues required for duplex recognition by an RNA-guided Cas12a.

The structure also reveals a fully formed DNA:RNA heteroduplex scaffolded by the REC lobe of Cas12a (Fig. 1c). This heteroduplex follows the same trajectory observed for an R-loop during canonical target recognition with the target RNA positioned where the crRNA is normally located. The noncomplementary region of the 40-nt ssRNA target exits the structure at the interface of the WED and RuvC domains, where the crRNA hairpin would be expected to form in a canonical Cas12a structure. As this region in the target RNA was designed to contain no secondary structure, it is not resolved in the cryo-EM reconstruction.

[1]Department of Molecular Biosciences, University of Texas at Austin, Austin, TX, USA. [2]Interdisciplinary Life Sciences Graduate Programs, University of Texas at Austin, Austin, TX, USA. [3]Department of Chemical Engineering, University of Florida, Gainesville, FL, USA. [4]Department of Chemistry, University of Florida, Gainesville, FL, USA. [5]Department of Molecular Genetics and Microbiology, University of Florida, Gainesville, FL, USA. [6]UF Health Cancer Center, University of Florida, Gainesville, FL, USA. [7]Center for Systems and Synthetic Biology, University of Texas at Austin, Austin, TX, USA. [8]LIVESTRONG Cancer Institutes, Dell Medical School, University of Texas at Austin, Austin, TX, USA. [9]These authors contributed equally: Rodrigo Fregoso Ocampo, Carlos Orosco. ✉e-mail: Jainp@ufl.edu; dtaylor@utexas.edu

https://doi.org/10.1038/s41594-026-01894-5

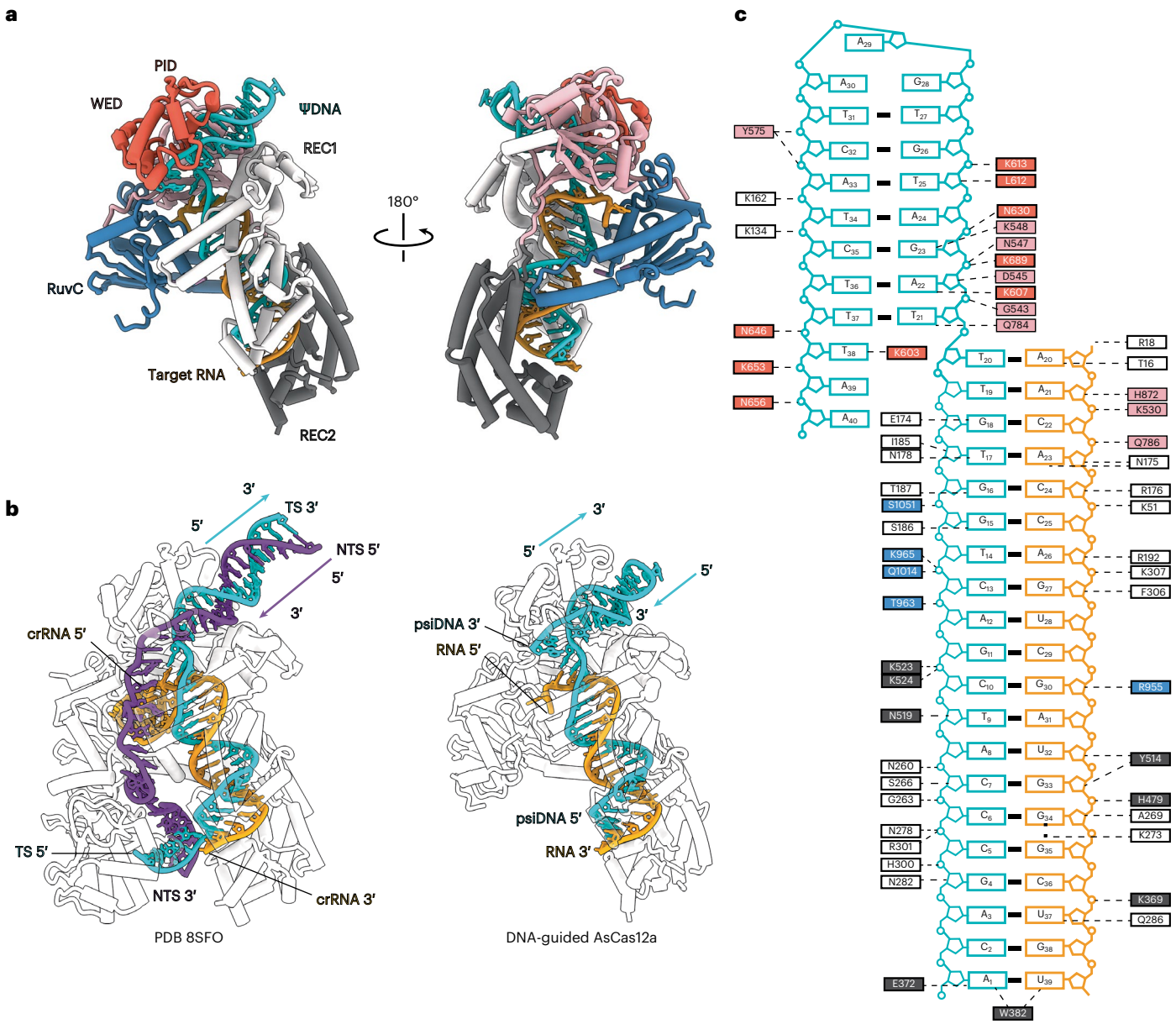


Fig. 1 | Structural basis for RNA targeting by ΨDNA-guided AsCas12a. a, Front and back views of the atomic model of ΨDNA-guided AsCas12a targeting a 40-nt target RNA (PDB 12YR). REC1 (snow), REC2 (dim gray), PID (tomato), WED (pink) and RuvC (steel blue) domains were resolved in the structure and modeled along with the ΨDNA (cyan) and target RNA (orange). **b**, Left, atomic model of a 20-bp AsCas12a effector targeting a canonical fully matched dsDNA duplex containing a canonical TTTN PAM (PDB 8SFO). The protein domains are transparent to allow visualization of the trajectory and directionality of the TS (cyan), NTS (dark orchid) and crRNA (orange). Right, AsCas12a atomic model bound to a ΨDNA targeting a 40-nt target RNA. The polarity of the ΨDNA is conserved compared to the TS and NTS of a canonical AsCas12a system. **c**, Overview of the contacts formed between AsCas12a and the DNA:RNA heteroduplex. Many of the contacts to this heteroduplex are conserved, including W382, which caps the PAM-distal end of the canonical R-loop after position 20. Notable contacts that are not formed are in the RuvC lid and bridge helix.

The region of Cas12a that recognizes the crRNA hairpin was, likewise, not resolved in the structure. This flexibility is consistent with the absence of stabilizing interactions normally provided by the crRNA handle but consistent with previous reports that Cas12a can function with noncanonical crRNAs[13]. These observations indicate that DNA-guided RNA targeting preserves the canonical hybrid nucleic acid-binding of Cas12a along the spacer region.

A canonical PAM-containing ΨDNA enhances target recognition

Cas12a bends the ΨDNA hairpin to enable PAM-analogous contacts by amino acids previously characterized to recognize a 5′ TTTN PAM in a canonical dsDNA target duplex[14]. The ΨDNA contains residues that would correspond to a TCTT PAM. The presence of pyrimidines at positions −2 to −4 enables the hairpin to acquire a geometry like that acquired by a canonical PAM. This enables AsCas12a to stabilize the hairpin using base-specific contacts between T38 and K603 and between G23 and K548, respectively, previously shown to be important in PAM recognition. The interaction between Cas12a and ΨDNA is further stabilized by a contact between Q784 and the final base of the duplex, T21, which forms a noncanonical base pair with T37 (Fig. 2a). Substitutions of N630 and K689 significantly hindered the *trans*-cleavage activity of Cas12a, suggesting that backbone-specific contacts are important to engage and stabilize the DNA hairpin. Surprisingly, individual alanine

https://doi.org/10.1038/s41594-026-01894-5

Table 1 | Cryo-EM data collection, refinement and validation statistics

	ΨDNA-guided AsCas12a (EMD-76860), (PDB 12YR)
Data collection and processing	
Magnification	×150,000
Voltage (kV)	300
Electron exposure (e^- per Å^2)	79
Defocus range (μm)	1.5–2.5
Pixel size (Å)	0.833
Symmetry imposed	None
Initial particle images (no.)	963,667
Final particle images (no.)	296,277
Map resolution (Å)	3.18
FSC threshold	0.143
Map resolution range (Å)	2.97–4.31
Refinement	
Initial model used (PDB code)	8SFO
Model resolution (Å)	3.30
FSC threshold	0.143
Model resolution range (Å)	NA
Map sharpening *B* factor (Å^2)	NA
Model composition	
Nonhydrogen atoms	8,561
Protein residues	949
Nucleotide residues	61
Ligands	0
B factors (Å^2)	
Protein	87.97
Nucleotide	77.18
Ligand	NA
Root-mean-square deviations	
Bond lengths (Å)	0
Bond angles (°)	4
Validation	
MolProbity score	1.10
Clashscore	3.04
Poor rotamers (%)	0.72
Ramachandran plot	
Favored (%)	98.18
Allowed (%)	1.82
Disallowed (%)	0.00

FSC, Fourier shell correlation; NA, not applicable.

substitutions of amino acids that form base-specific contacts did not hinder AsCas12a *trans*-cleavage activity, indicating that AsCas12a can accommodate hairpins that do not contain a canonical PAM-analogous region (Fig. 2b). These interactions suggest that Cas12a recognizes the ΨDNA handle through a mechanism analogous to PAM binding but can tolerate deviations from canonical base pairing, provided that the overall duplex geometry is preserved.

It has been shown that PAM binding contributes to R-loop formation by enabling PAM-proximal bases of dsDNA to flip or twist to probe the single guide RNA for complementarity[15]. As our ΨDNA design contains a single-stranded DNA (ssDNA) adjacent to the PAM and does not require this mechanism to occur to form a productive heteroduplex, we hypothesized that PAM recognition might not be strictly required in ΨDNA-guided AsCas12a, despite observing multiple conserved contacts. To test this, we flipped the bases of the hairpin of the ΨDNA to maintain hairpin stability, while simultaneously changing the region analogous to the PAM. This engineered PAM-analogous region was designed to contain a purine-rich AGAT sequence, which diverges substantially from the TTTN PAM AsCas12a usually requires for activation. This ΨDNA design still showed significant *trans*-cleavage activity, despite a ~3-fold reduction, indicating that ΨDNA can still accommodate a handle that is very different from the canonical PAM (Fig. 2c). Together, these results show that a pyrimidine-rich ΨDNA PAM-analogous region enhances the *trans*-cleavage activity of Cas12a but Cas12a can still accommodate other sequences if a stable hairpin is present. It is tempting to hypothesize that rationally designing changes to the ΨDNA sequence could lead to tunable activity.

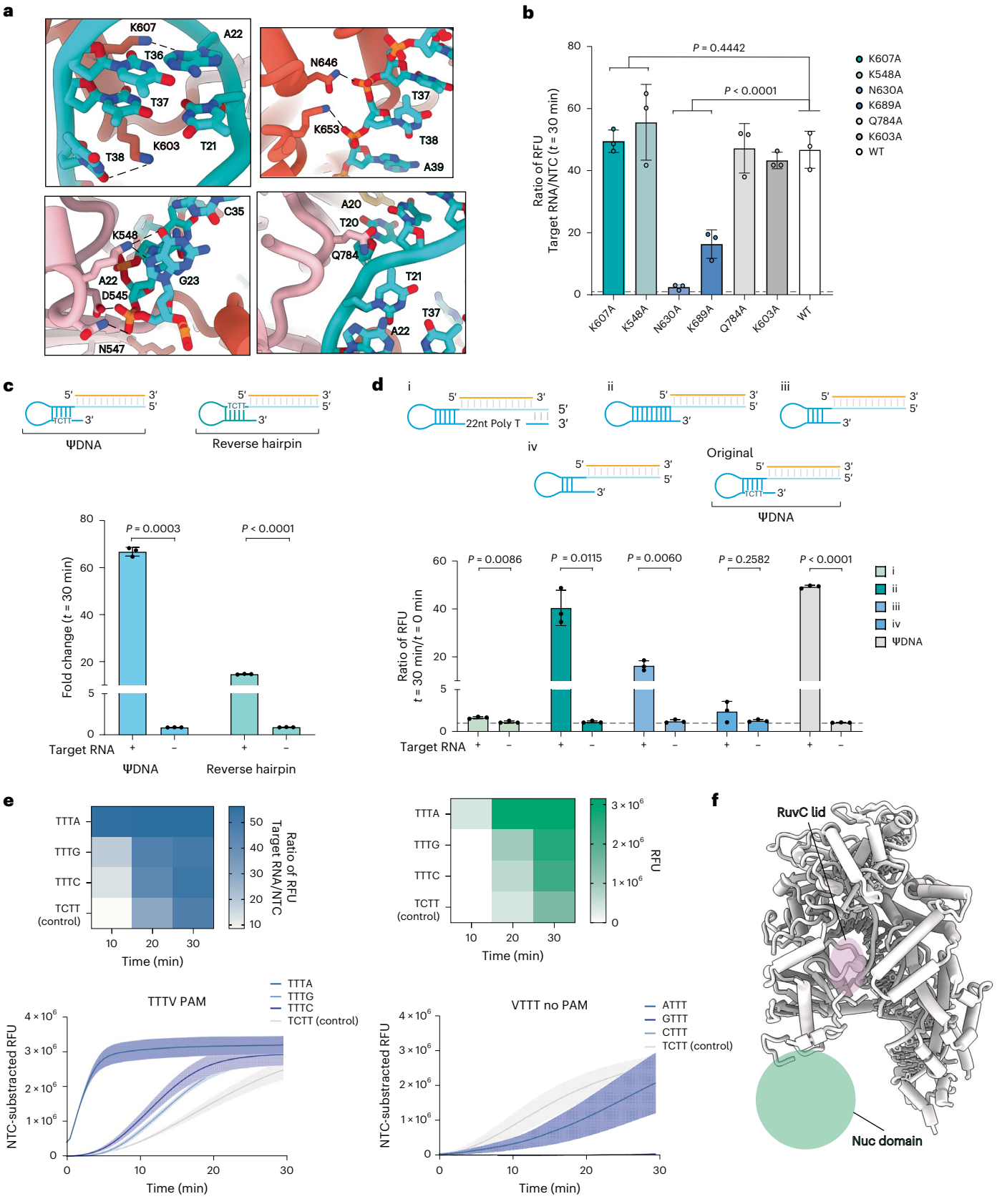
To test whether the canonical PAM would yield more efficient RNA detection, we modified the ΨDNA hairpin to contain PAMs for AsCas12a. Although endpoint measurements showed a similar level of activity for all PAMs when compared to the control TCTT PAM (Fig. 2d), performing a time-course assay revealed that Cas12a achieves significantly faster rates of *trans*-cleavage when a TTTA PAM-analogous hairpin is used, followed by TTTG and TTTC. Even though Cas12a was still able to exhibit *trans*-cleavage activity on VTTT (no PAM) ΨDNA, *trans*-cleavage occurred at a significantly slower rate (Fig. 2e). Overall, these results support a mechanism where Cas12a recognition of the ΨDNA is rate limiting and can be tuned by architecture and sequence.

The DNA spacer region follows the standard trajectory that the DNA TS would follow in the presence of a fully matched DNA duplex. This similarity suggests that the protein primarily recognizes the hybrid duplex through nonspecific backbone interactions rather than strict nucleic acid identity. However, given that the ΨDNA is only 41 bp, the region that would be considered analogous to the non-TS (NTS) is incomplete and, therefore, only the first three bases (ΨDNA 38–40) are present in the structure. This region stabilizes the PAM-interacting domain by forming multiple contacts along its positively charged surface instead of forming a pseudoknot characterized in AsCas12a crRNA. These interactions partially compensate for the absence of the extended NTS normally present during DNA targeting. In a canonical AsCas12a structure, the remainder of the NTS partitions through the RuvC and Nuc domains, enabling RuvC lid formation and R-loop maturation[16,17]. However, our structure reveals that, without an NTS, both the RuvC lid and the Nuc lobes are unresolved (Fig. 2f). This observation indicates that stabilization of these domains depends on interactions with the displaced NTS. Because the RuvC lid is not present, multiple contacts with the TS, previously characterized in a 20-bp R-loop complex, are not present in the structure, including stabilizing contacts by K965 and Q1013 (ref. 11). While the active-site residues of AsCas12a are exposed, the RuvC lid is disordered and not in the α-helical conformation required for cleavage, likely because of the lack of a nucleic acid substrate for engagement (Extended Data Fig. 2). Despite this, AsCas12a is still able to stably bind a fully formed double-stranded duplex with a fully docked bridge helix and REC2 domain, as evidenced by the presence of W382 capping the PAM-distal end of the R-loop[18,19].

Discussion

Together, these findings reveal how Cas12a can accommodate DNA-guided RNA recognition through structural mimicry of canonical CRISPR nucleic acid components. Interestingly, these results are also consistent with a recent study that used AlphaFold to model DNA-guided Cas12a for RNA targeting[20]. The ΨDNA hairpin recreates the geometry of the PAM-proximal duplex and is stabilized by interactions with the PAM-interacting domain, while the spacer region forms

https://doi.org/10.1038/s41594-026-01894-5



a canonical RNA–DNA heteroduplex within the REC lobe. The absence of a complete NTS alters the conformation of nuclease-domain elements associated with cleavage activation, highlighting the structural plasticity of Cas12a in accommodating alternative nucleic acid substrates. This structure provides a framework for understanding DNA-guided RNA-targeting Cas enzymes and offers insights that may guide the engineering of CRISPR systems for programmable RNA detection and manipulation beyond Cas12 systems[13]. More broadly, this structural framework expands the potential targeting modalities of CRISPR nucleases.

Fig. 2 | ΨDNA hairpin mimics PAM binding. a, Visualization of PAM-analogous contacts formed between AsCas12a and the ΨDNA hairpin. K607 and Q784 form base-specific contacts with A22 and T37, respectively, while D545 and N547 in the WED domain form stabilizing contacts with the phosphate backbone of the ΨDNA. In addition, K603 is intertwined with the end of the ΨDNA handle and contacts T38. N646 and K653 stabilize the phosphate backbone of the NTS-analogous end through nonspecific contacts with the phosphate backbone. **b**, *Trans*-cleavage assay of individual Cas12a alanine substitutions, focusing on residues that either contact the phosphate backbone of the ΨDNA or form base-specific contacts in the PAM-analogous region. The fold change in relative fluorescence units (RFU) was used to monitor *trans*-cleavage activity. An increase in fluorescence signal occurs when the ssDNA probe containing both a fluorophore and a quencher is cleaved. Data represent the mean ± s.d. ($n = 3$ independent replicates). Statistical significance between the sample with target RNA and nontarget RNA control (NTC) was determined using a one-way analysis of variance. $P = 0.4442$ for WT, K607A and K548A; $P < 0.0001$ across all samples. **c**, *Trans*-cleavage assays using AsCas12a bound to a standard ΨDNA guide with a TCTT PAM and reverse hairpin ΨDNA guide containing a AGAT PAM. Error bars represent the mean ± s.d. ($n = 3$ independent experiments). Statistical significance was evaluated using two-sided unpaired *t*-tests. $P = 0.0003$ for ΨDNA guide with a TCTT PAM and $P < 0.0001$ for the reverse hairpin. **d**, *Trans*-cleavage assays using multiple ΨDNA designs, including elongated and shortened hairpins or with an extended NTS. Data represent the mean ± s.d. ($n = 3$ independent replicates). Statistical significance was evaluated using two-sided unpaired *t*-tests. (i) $P = 0.0086$, (ii) $P = 0.0115$, (iii) $P = 0.0060$, (iv) $P = 0.2582$ and (Ψ) $P < 0.0001$. **e**, *Trans*-cleavage rates of AsCas12a incubated with ΨDNA guides containing different PAM-analogous regions, including canonical PAMs (left) and noncanonical PAMs (right). The plots indicate that canonical PAMs enable faster *trans*-cleavage rates, as opposed to the slower *trans*-cleavage rates observed when using ΨDNAs with noncanonical PAMs. The solid line represents the mean and the shaded region represents the s.d. ($n = 3$ independent experiments). **f**, Front view of the atomic model of ΨDNA-guided AsCas12a (PDB 12YR), with transparent regions indicating the missing Nuc lobe (green) and bride helix (plum).

Online content

Any methods, additional references, Nature Portfolio reporting summaries, source data, extended data, supplementary information, acknowledgements, peer review information; details of author contributions and competing interests; and statements of data and code availability are available at https://doi.org/10.1038/s41594-026-01894-5.

References

1. Broughton, J. P. et al. CRISPR–Cas12-based detection of SARS-CoV-2. *Nat. Biotechnol.* **38**, 870–874 (2020).
2. Ran, F. A. et al. Genome engineering using the CRISPR–Cas9 system. *Nat. Protoc.* **8**, 2281–2308 (2013).
3. Zetsche, B. et al. Cpf1 is a single RNA-guided endonuclease of a class 2 CRISPR–Cas system. *Cell* **163**, 759–771 (2015).
4. Swarts, D. C. & Jinek, M. Mechanistic insights into the *cis*- and *trans*-acting DNase activities of Cas12a. *Mol. Cell* **73**, 589–600 (2019).
5. Dmytrenko, O. et al. Cas12a2 elicits abortive infection through RNA-triggered destruction of dsDNA. *Nature* **613**, 588–594 (2023).
6. Dmytrenko, O. et al. RNA-triggered Cas12a3 cleaves tRNA tails to execute bacterial immunity. *Nature* **649**, 1312–1321 (2026).
7. Rananaware, S. R. et al. Programmable RNA detection with CRISPR–Cas12a. *Nat. Commun.* **14**, 5409 (2023).
8. East-Seletsky, A. et al. Two distinct RNase activities of CRISPR–C2c2 enable guide-RNA processing and RNA detection. *Nature* **538**, 270–273 (2016).
9. Orosco, C. et al. DNA-guided CRISPR–Cas12 for RNA targeting. *Nat. Biotechnol.* https://doi.org/10.1038/s41587-026-03129-w (2026).
10. Swarts, D. C., van der Oost, J. & Jinek, M. Structural basis for guide RNA processing and seed-dependent DNA targeting by CRISPR–Cas12a. *Mol. Cell* **66**, 221–233.e4 (2017).
11. Strohkendl, I. et al. Cas12a domain flexibility guides R-loop formation and forces RuvC resetting. *Mol. Cell* **84**, 2717–2731 (2024).
12. Yamano, T. et al. Structural basis for the canonical and non-canonical PAM recognition by CRISPR–Cpf1. *Mol. Cell* **67**, 633–645 (2017).
13. Nguyen, L. T. et al. Harnessing noncanonical crRNAs to improve functionality of Cas12a orthologs. *Cell Rep.* **43**, 113777 (2024).
14. Soczek, K. M., Cofsky, J. C., Tuck, O. T., Shi, H. & Doudna, J. A. CRISPR–Cas12a bends DNA to destabilize base pairs during target interrogation. *Nucleic Acids Res.* **53**, gkae1192 (2025).
15. Cofsky, J. C., Soczek, K. M., Knott, G. J., Nogales, E. & Doudna, J. A. CRISPR–Cas9 bends and twists DNA to read its sequence. *Nat. Struct. Mol. Biol.* **29**, 395–402 (2022).
16. Saha, A. et al. An alpha-helical lid guides the target DNA toward catalysis in CRISPR–Cas12a. *Nat. Commun.* **15**, 1473 (2024).
17. Ganguly, C. et al. Bridge helix of Cas12a is an allosteric regulator of R-loop formation and RuvC activation. *Nat. Commun.* **17**, 2126 (2026).
18. Naqvi, M. M., Lee, L., Montaguth, O. E. T., Diffin, F. M. & Szczelkun, M. D. CRISPR–Cas12a-mediated DNA clamping triggers target-strand cleavage. *Nat. Chem. Biol.* **18**, 1014–1022 (2022).
19. Parameshwaran, H. P. et al. The bridge helix of Cas12a imparts selectivity in *cis*-DNA cleavage and regulates *trans*-DNA cleavage. *FEBS Lett.* **595**, 892–912 (2021).
20. Wu, X. et al. DNA-guided CRISPR–Cas12a effectors for programmable RNA recognition and cleavage. *Nat. Biotechnol.* https://doi.org/10.1038/s41587-026-03120-5 (2026).

Publisher's note Springer Nature remains neutral with regard to jurisdictional claims in published maps and institutional affiliations.

Open Access This article is licensed under a Creative Commons Attribution-NonCommercial-NoDerivatives 4.0 International License, which permits any non-commercial use, sharing, distribution and reproduction in any medium or format, as long as you give appropriate credit to the original author(s) and the source, provide a link to the Creative Commons licence, and indicate if you modified the licensed material. You do not have permission under this licence to share adapted material derived from this article or parts of it. The images or other third party material in this article are included in the article's Creative Commons licence, unless indicated otherwise in a credit line to the material. If material is not included in the article's Creative Commons licence and your intended use is not permitted by statutory regulation or exceeds the permitted use, you will need to obtain permission directly from the copyright holder. To view a copy of this licence, visit http://creativecommons.org/licenses/by-nc-nd/4.0/.

© The Author(s) 2026

https://doi.org/10.1038/s41594-026-01894-5

Methods

Plasmid design and cloning

An AsCas12a protein was codon-optimized for expression in *Escherichia coli* and its DNA sequence was cloned into a pET28 expression vector under *lacO* repression with a 6× N-terminal His tag and a tobacco etch virus (TEV) protease using the NEBridge Golden Gate buffer set (New England Biolabs) and following manufacturer's instructions.

Oligonucleotide sequences

ΨDNA:
ACAGCCCATCGACTGGTGTTTAGATGTGAATCATCTTTAAT;
ΨDNA reverse hairpin:
ACAGCCCATCGACTGGTGTTTTCTACTAAGTGTAGATTAAT;
miR-21 RNA:
rGrArCrArUrUrUrArArCrArArCrArCrCrArGrUrCrGrArUrGrGrGrCrUrGrUrArGrCrArUrArA rArGrU;
ΨDNA-21 (i):
GAGACAGCCCATCGACTGGTGTTTAGATGTGAATCATCTTTTTTTTTTTTTTTTTTTTTTTCTC;
ΨDNA-21 (ii):
ACAGCCCATCGACTGGTGTTTAGATGCCCTGAATGGGCATCTTTAAT;
ΨDNA-21 (iii):
ACAGCCCATCGACTGGTGTTTAGATTGAATATCTTTAAT;
ΨDNA-21 (iv):
ACAGCCCATCGACTGGTGTTTAGATGAATTCTTTAAT;
ΨDNA-21 TTTA:
ACAGCCCATCGACTGGTGTTTAAATGTGAATCATTTATAAT;
ΨDNA-21 TTTG:
ACAGCCCATCGACTGGTGTTTAAATGTGAATCATTTGTAAT;
ΨDNA-21 TTTC:
ACAGCCCATCGACTGGTGTTTAAATGTGAATCATTTCTAAT;
ΨDNA-21 ATTT:
ACAGCCCATCGACTGGTGTTTAAATGTGAATCATATTTAAT;
ΨDNA-21 GTTT:
ACAGCCCATCGACTGGTGTTTAAATGTGAATCATGTTTAAT;
ΨDNA-21 CTTT:
ACAGCCCATCGACTGGTGTTTAAATGTGAATCATCTTTAAT.

Protein expression and purification

All proteins were purified as previously described[11]. In brief, the cloned AsCas12a pET28 expression plasmid was transformed into BL21 DE3 chemically competent cells (New England Biolabs) and plated under kanamycin selection. A single colony was inoculated into 50 ml of Luria–Bertani (LB) under kanamycin antibiotic selection and allowed to grow at 37 °C for 16 h. The inoculate was then back diluted 1:100-fold into two separate 1.5-L LB culture flasks and grown to an optical density at 600 nm of 0.8. Expression was induced by the addition of IPTG at a final concentration of 0.1 mM and growth for 16 h at 18 °C to maximize expression levels. Cells were pelleted by centrifugation (4,000*g*, 60 min) and resuspended using lysis buffer (20 mM Tris-HCl pH 7.5, 1 M NaCl, 10 mM $MgCl_2$, 1 mM TCEP, 200 µM PMSF and 10% glycerol) with one Pierce protease inhibitor tablet and 10 U of DNAse I. Cells were lysed by sonication and the lysate was clarified by centrifugation at 18,000*g* for 30 min at 4 °C. The supernatant was loaded into a 5-ml HisTrap HP Ni Column (Cytiva) and eluted using a gradient of Ni elution buffer (20 mM Tris-HCl pH 8.0, 500 mM NaCl, 250 mM imidazole, 1 mM TCEP and 10% glycerol). Fractions containing the protein were combined and dialyzed with TEV protease in dialysis buffer (40 mM HEPES pH 7.5, 150 mM NaCl, 1 mM TCEP and 10% glycerol) for 16 h at 4 °C. The sample was then purified by gel-filtration chromatography (Superose 6 10/300; GE Healthcare) in dialysis buffer. The purity and quality of the protein were analyzed by SDS–PAGE. The protein was quantified using the PIERCE Bradford assay reagent kit (Thermo Fisher) following the manufacturer's instructions. The protein was flash-frozen in 6-µl aliquots at a final concentration of 70.5 µM and stored at −80 °C.

In vitro *trans*-cleavage assay

The ΨDNA–AsCas12 *trans*-cleavage assays were prepared at 50 nM AsCas12a enzyme, 100 nM ΨDNA, 40 nM target RNA and 500 nM FQ ssDNA reporter. All components were added in NEB 2.1 buffer and nuclease-free water at a final volume of 40 µl. Then, all reactions were plated on a dark flat-bottom 384-well plate (Grenier) and subsequently placed in a BioTek Synergy fluorescence microplate reader. Samples were incubated at a temperature of 37 °C for 30 min. Fluorescence was recorded at 483/20 nm and 530/20 nm excitation/emission wavelengths in 2.5-min intervals.

Cryo-EM sample preparation and data collection

Samples were prepared and imaged following previously described procedures[11]. In brief, for the 20-bp complex, a flash-frozen sample of purified AsCas12a was rapidly thawed and incubated at a 10 µM final concentration with ΨDNA (purified by high-performance liquid chromatography)containing an miR-21-targeting spacer at a 1:1 ratio at 37 °C for 30 min. After a 30-min incubation, a 40-nt target RNA containing a region complementary to the miR-21-targeting spacer was added at a final concentration of 10 µM and further incubated for 30 min at 37 °C. The sample was then allowed to cool on ice before being applied to Quantifoil 1.2/1.3 ultrathin 400-mesh carbon grids that were glow-discharged with 20 mA for 30 s before blotting. All grids were blotted using a Vitrobot Mark IV (Thermo Fisher) for 9–12 s (blot force: 1) at 4 °C and 100% humidity and plunge-frozen in liquid ethane. Data were collected on an FEI Titan Krios 300-V Transmission EM instrument (Thermo Scientific) with a Gatan BioContinuum imaging filter and a K3 direct electron detector. Data were collected using SerialEM (version 4.2) with a 0.832-Å pixel size and a defocus range of −1.5 to −2.5 µm, with a total exposure time of 3.3 s in a total accumulated dose of 79 e^- per $Å^2$ at −30° tilt. Motion correction, contrast transfer function estimation and particle picking were carried out in cryoSPARC live (version 4.7.1). A total of 4,338 videos were accepted for downstream processing.

Cryo-EM image processing, model building and refinement

Similarly, the cryo-EM processing pipeline used was adapted from previously described procedures[11]. From the accepted videos, a total of 1,767,373 particles were selected using blob picker. A total of 1,107,909 particles were picked after a single round of two-dimensional classification. A random subset of 100,000 picked particles was selected for ab initio reconstruction (three classes). The best class was used for two rounds of heterogeneous refinement and downstream nonuniform refinement, yielding a 3.10-Å reconstruction comprising 963,667 particles. Given that the Nuc domain was mostly unresolved, particle homogeneity was enhanced by performing a single round of three-dimensional classification. All classes contained either a partially resolved or fully unresolved Nuc domain. Classes containing the fully unresolved Nuc domain were selected for a final nonuniform refinement, yielding a final 3.18-Å reconstruction comprising 296,227 particles.

Model building and refinement

As the structure resembled a fully formed 20-bp R-loop conformation, the initial backbone for the model was built using a previously solved structure (PDB 8SFO) and aligning it to the map. The alignment yielded a well-aligned DNA:RNA heteroduplex, as well as the α-helices from the protein. The output was used as a fiducial for de novo model building using a combination of Coot (version 1.0) and ChimeraX (version 1.90). The DNA NTS was deleted from the map along with the Nuc domain. The DNA hairpin was modeled manually using Isolde (version 1.4). Side-chain rotamer optimization and Ramachandran angle refinement

were performed using a combination of Coot (version 1.0) and Isolde (version 1.4). Multiple iterations of real-space refinement implemented within PHENIX (version 1.19) were carried out to improve the model geometry and map fit.

Reporting summary

Further information on research design is available in the Nature Portfolio Reporting Summary linked to this article.

Data availability

All data supporting the findings of this study are available within the article. Additional data can be obtained from the corresponding authors, D.W.T. or P.K.J., upon reasonable request. The atomic coordinates were deposited to the Protein Data Bank (PDB) under accession code 12YR. The cryo-EM density map was deposited to the Electron Microscopy Data Bank (EMDB) under accession code EMD-76860. Source data are provided with this paper.

Acknowledgements

We extend our gratitude to the University of Texas Austin and the University of Florida Health Cancer Center for their support. We also thank the members of the D.W.T. and P.K.J. labs for valuable discussions and for their help with experiments.

Author contributions

R.F.O. and M.W. performed the cryo-EM structure determination, model building and structural analysis. R.F.O. and C.O. purified and reconstituted the enzyme complexes, while C.O., B.H. and B.P. conducted the biochemical experiments. Data analysis and interpretation and manuscript preparation were performed by R.F.O., C.O., P.K.J. and D.W.T. P.K.J. and D.W.T. supervised the study and secured funding.

Funding

This work was funded by the Exxon Mobil Gator Alumni Faculty and Shah Foundation Endowment Funds (P.K.J.) and by the National Institutes of Health through the National Institute of Allergy and Infectious Diseases (R61AI181016, to P.K.J.) and the National Institute of General Medical Sciences (R35GM147788, to P.K.J.; R35GM158551, to D.W.T.). Computational resources for this work were supported by Welch Foundation grant F-1938 (D.W.T.). The funding sources had no role in study design, data collection, analysis, interpretation or manuscript preparation.

Competing interests

C.O., B.H. and P.K.J., are listed as inventors on a patent application related to the content of this work. P.K.J. is a cofounder of CasNx, Inc. and CRISPR, LLC. The remaining authors declare no competing interests.

Additional information

Extended data is available for this paper at https://doi.org/10.1038/s41594-026-01894-5.

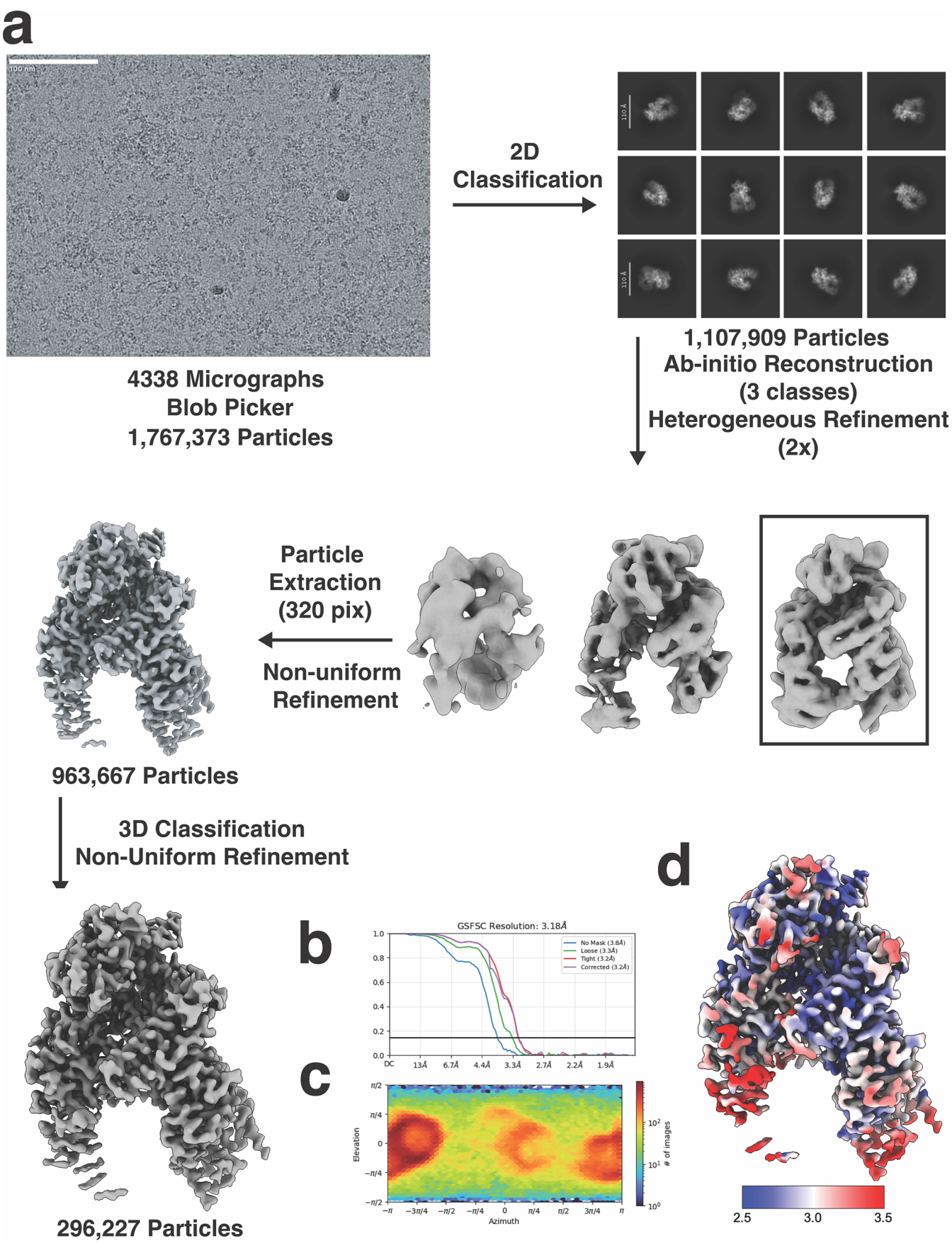
Supplementary information The online version contains supplementary material available at https://doi.org/10.1038/s41594-026-01894-5.

Correspondence and requests for materials should be addressed to Piyush K. Jain or David W. Taylor.

Peer review information *Nature Structural & Molecular Biology* thanks the anonymous reviewer(s) for their contribution to the peer review of this work. Peer reviewer reports are available.

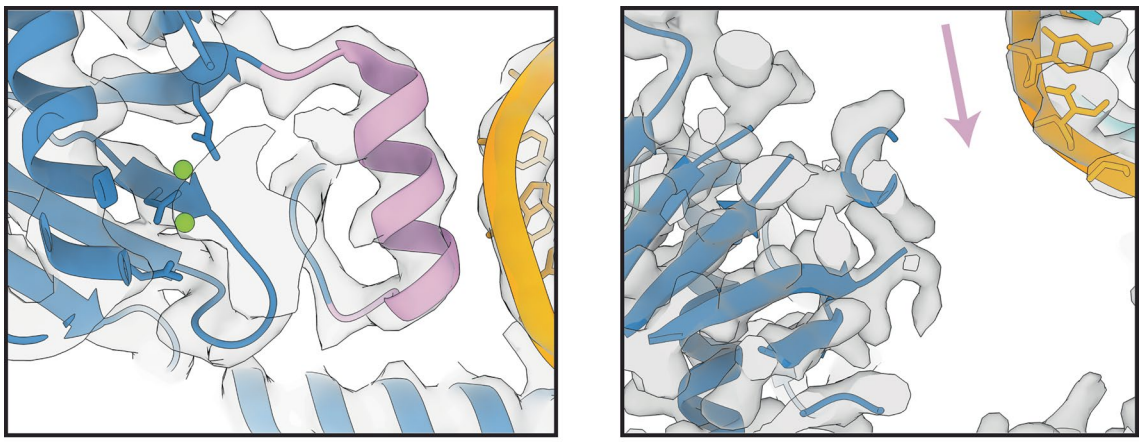
Reprints and permissions information is available at www.nature.com/reprints.

https://doi.org/10.1038/s41594-026-01894-5



Extended Data Fig. 1 | Cryo-EM dataset processing pipeline, data analysis and quality control. a. Processing pipeline for ΨDNA-guided RNA targeting AsCas12a. **b**. Fourier Shell Correlation (FSC) diagram for the final cryo-EM structure obtained. **c**. Euler particle distribution diagram shows a well-represented orientation distribution of particles for the final cryo-EM structure. **d**. Sharpened map colored by local resolution with gold-standard FSC at a threshold of 0.143.

https://doi.org/10.1038/s41594-026-01894-5



Extended Data Fig. 2 | Comparison of the RuvC lid active site. (Left) Front view of the model and map showing a fully resolved RuvC lid (PDB: 8SFO). (Right) Front view of the model and map of ΨDNA-guided AsCas12a. The density corresponding to the RuvC lid is not present in the map as indicated by the arrow.

nature portfolio

Corresponding author(s): David W. Taylor

Last updated by author(s): 8/24/2026

Reporting Summary

Nature Portfolio wishes to improve the reproducibility of the work that we publish. This form provides structure for consistency and transparency in reporting. For further information on Nature Portfolio policies, see our Editorial Policies and the Editorial Policy Checklist.

Statistics

For all statistical analyses, confirm that the following items are present in the figure legend, table legend, main text, or Methods section.

n/a	Confirmed	
☐	☒	The exact sample size (*n*) for each experimental group/condition, given as a discrete number and unit of measurement
☐	☒	A statement on whether measurements were taken from distinct samples or whether the same sample was measured repeatedly
☐	☒	The statistical test(s) used AND whether they are one- or two-sided *Only common tests should be described solely by name; describe more complex techniques in the Methods section.*
☒	☐	A description of all covariates tested
☒	☐	A description of any assumptions or corrections, such as tests of normality and adjustment for multiple comparisons
☐	☒	A full description of the statistical parameters including central tendency (e.g. means) or other basic estimates (e.g. regression coefficient) AND variation (e.g. standard deviation) or associated estimates of uncertainty (e.g. confidence intervals)
☐	☒	For null hypothesis testing, the test statistic (e.g. *F*, *t*, *r*) with confidence intervals, effect sizes, degrees of freedom and *P* value noted *Give P values as exact values whenever suitable.*
☒	☐	For Bayesian analysis, information on the choice of priors and Markov chain Monte Carlo settings
☒	☐	For hierarchical and complex designs, identification of the appropriate level for tests and full reporting of outcomes
☒	☐	Estimates of effect sizes (e.g. Cohen's *d*, Pearson's *r*), indicating how they were calculated

Our web collection on statistics for biologists contains articles on many of the points above.

Software and code

Policy information about availability of computer code

Data collection	Data were collected on an FEI Titan Krios 300 V Transmission Electron Microscope (Thermo Scientific) with a Gatan BioContinuum Imaging Filter and a K3 direct electron detector. Data were collected using Serial EM v4.2 with a 0.832 Å pixel size and a defocus range of –1.5 to –2.5 µm with a total exposure time of 3.3 s in a total accumulated dose of 79e/A2 at -30° tilt. Motion correction, contrast transfer function (CTF) estimation, and particle picking were carried out in cryoSPARC live v4.7.1.
Data analysis	All subsequent data processing was carried out in cryoSPARC v4.4. PDB: 8SFO was fit in the reconstruction as a rigid body in ChimeraX. The DNA hairpin was modeled manually using Isolde v1.4. The whole model was manually refined in COOT, and automatically refined by real_space_refine in PHENIX. All structural figures were generated using ChimeraX v1.7.1.

For manuscripts utilizing custom algorithms or software that are central to the research but not yet described in published literature, software must be made available to editors and reviewers. We strongly encourage code deposition in a community repository (e.g. GitHub). See the Nature Portfolio guidelines for submitting code & software for further information.

Data

Policy information about availability of data

All manuscripts must include a data availability statement. This statement should provide the following information, where applicable:

- Accession codes, unique identifiers, or web links for publicly available datasets
- A description of any restrictions on data availability
- For clinical datasets or third party data, please ensure that the statement adheres to our policy

All the data supporting the findings of this study are available within the Article and Supplementary Files. Additional data can be obtained from the corresponding authors, D.W.T. or P.K.J., upon reasonable request. The atomic coordinates have been deposited in the Protein Data Bank under accession code PDB YYYY. The cryo-EM structure has been deposited in the Electron Microscopy Data Bank under accession code EMD-ZZZZ.

Research involving human participants, their data, or biological material

Policy information about studies with human participants or human data. See also policy information about sex, gender (identity/presentation), and sexual orientation and race, ethnicity and racism.

Reporting on sex and gender	Not applicable.
Reporting on race, ethnicity, or other socially relevant groupings	Not applicable.
Population characteristics	Not applicable.
Recruitment	Not applicable.
Ethics oversight	Not applicable.

Note that full information on the approval of the study protocol must also be provided in the manuscript.

Field-specific reporting

Please select the one below that is the best fit for your research. If you are not sure, read the appropriate sections before making your selection.

☒ Life sciences ☐ Behavioural & social sciences ☐ Ecological, evolutionary & environmental sciences

For a reference copy of the document with all sections, see nature.com/documents/nr-reporting-summary-flat.pdf

Life sciences study design

All studies must disclose on these points even when the disclosure is negative.

Sample size	A sample size of three independent biological replicates were chosen to derive statistical measurements.
Data exclusions	No data was excluded.
Replication	All experiments were replicated at least three times with similar results.
Randomization	Particle orientations are randomized during processing.
Blinding	No blinding was performed. The experiments were observational and not subject to bias.

Reporting for specific materials, systems and methods

We require information from authors about some types of materials, experimental systems and methods used in many studies. Here, indicate whether each material, system or method listed is relevant to your study. If you are not sure if a list item applies to your research, read the appropriate section before selecting a response.

Materials & experimental systems

n/a	Involved in the study
☒	☐ Antibodies
☒	☐ Eukaryotic cell lines
☒	☐ Palaeontology and archaeology
☒	☐ Animals and other organisms
☒	☐ Clinical data
☒	☐ Dual use research of concern
☒	☐ Plants

Methods

n/a	Involved in the study
☒	☐ ChIP-seq
☒	☐ Flow cytometry
☒	☐ MRI-based neuroimaging

Plants

Seed stocks	Not applicable.
Novel plant genotypes	Not applicable.
Authentication	Not applicable.